Supplemental Material: Elastic Scattering Time of Matter-Waves in Disordered Potentials

Jérémie Richard,[1] Lih-King Lim,[2,1] Vincent Denechaud,[1,3] Valentin V. Volchkov,[1,4] Baptiste Lecoutre,[1] Musawwadah Mukhtar,[1] Fred Jendrzejewski,[1,5] Alain Aspect,[1] Adrien Signoles,[1] Laurent Sanchez-Palencia,[6] and Vincent Josse[1,*]

[1] *Laboratoire Charles Fabry, Institut d'Optique, CNRS, Université Paris-Saclay, 91127 Palaiseau cedex, France*
[2] *Zhejiang Institute of Modern Physics, Zhejiang University, Hangzhou 310027, P. R. China*
[3] *SAFRAN Sensing Solutions, Safran Tech, Rue des Jeunes Bois, Châteaufort CS 80112, 78772 Magny-les-Hameaux, France*
[4] *Max-Planck-Institute for Intelligent Systems, Max-Plack-Ring, 4, 72076 Tübingen, Germany*
[5] *Heidelberg University, Kirchhoff-Institut für Physik, Im Neuenheimer Feld 227, 69120 Heidelberg, Germany*
[6] *CPHT, Ecole Polytechnique, CNRS, Université Paris-Saclay, Route de Saclay, 91128 Palaiseau, France*

We describe here the methods (i) to extract the scattering time from the measurement, (ii) to generate and characterize the laser speckle field, (iii) to calculate the Born prediction adapted to our configuration and (iv) to perform the numerical simulations to estimate the scattering times.

EXTRACTION OF THE SCATTERING TIME τ_s

The measurement of the elastic scattering time τ_s is based on the decay of the initial momentum distribution $n(\mathbf{k}_i, t)$, as illustrated in Fig. **??** for the parameters $k_i = 2.31\sigma^{-1}$ and $V_R/h = -104\,\mathrm{Hz}$ (same as in Fig.2(a) on the main text).

The determination of τ_s is performed in three steps. First, we determine the angular profile $n(\theta, t)$ by radially integrating the momentum distribution $n(\mathbf{k}, t)$ in the (k_y, k_z) plane, $\theta = 0$ corresponding to the initial direction [Fig. **??**(a)]. The lower and upper integration limits correspond to twice the radial width of the initial momentum distribution. The reduced angular profile $\tilde{n}(\theta, t) = n(\theta, t)/n(0, 0)$ is obtained by normalizing this profile by its initial value at time $t = 0$ and $\theta = 0$. A typical angular profile $\tilde{n}(\theta, t)$ for $t = 17.5\,\mathrm{ms}$ is plotted on Fig.**??**(b) (blue line). The general shape results from the sum of two contributions: a narrow peak $\tilde{n}_i(\theta, t)$ that corresponds to the unscattered initial distribution and a broad background $\tilde{n}_b(\theta, t)$. The latter corresponds to the scattered atoms to direction $\mathbf{k}'$ and builds up progressively on time.

In a second step, the normalized height $\tilde{n}_i(t) = \tilde{n}_i(0, t)$ of the initial distribution is extracted by adjusting the bi-modal distribution by the sum of a narrow Gaussian peak accounting for $\tilde{n}_i(\theta, t)$ [**?**] and a broad Gaussian peak accounting for the background $\tilde{n}_b(\theta, t)$ [red solid line in Fig.**??**(b)]. Error bars of $\tilde{n}_i(t)$ represent one standard deviations and are estimated from the noise on the experimental data and the deviation of the model.

To finally extract τ_s, the decay of $\tilde{n}_i(t)$ is plotted in a semi-logarithmic scale [dots in Fig. **??**(c)] and then adjusted by a pure exponential law of typical time τ_s.

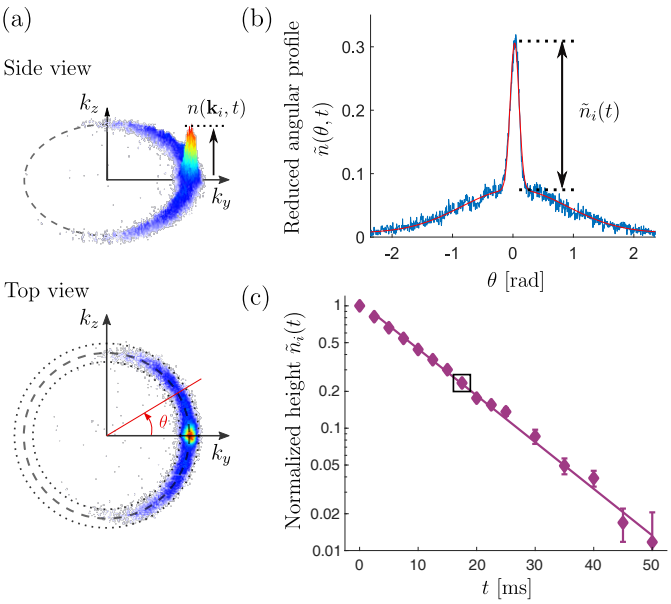

FIG. 1. **Measurement protocol of the scattering time τ_s.** The procedure is illustrated for the same parameters than in Fig. 2(a) of the main text, i.e., $k_i = 2.31\sigma^{-1}$ and $V_R = -104\,\mathrm{Hz}$. (a) Observed momentum distribution $n(\mathbf{k}, t)$ after a propagation time $t = 17.5\,\mathrm{ms}$ in the disorder (top: side view; bottom: top view). The angular profile is obtained by radially integrating around the initial peak (between the two dotted lines). (b) The reduced angular profile $\tilde{n}(\theta, t)$ (blue line) is adjusted by the sum of a narrow and a broad Gaussian peak, both centered around $\theta = 0$ (red line). The amplitude of the narrow peak is used to extract the normalized height $\tilde{n}_i(t)$. (c) The normalized height $\tilde{n}_i(t)$ is plotted as a function of the propagation time t. The experimental points are fitted by an exponential function of the form e^{-t/τ_s}. Here we find $\tau_s = 12.0(3)\,\mathrm{ms}$.

LASER SPECKLE DISORDERED POTENTIAL

Quasi-2D laser speckle field generation

The laser speckle field is created by passing a laser beam of wavelength $\lambda \sim 780$ nm through a diffusive plate, the configuration being identical as the one described in Ref. [**?**]. As illustrated in Fig. **??**(a), the incoming wave that illuminates the diffusive plate is converging at the position $d = 15.2(5)$ mm that coincides with the position of the atoms. The intensity profile of the illumination on the diffusive plate is a Gaussian shape, of waist $w = 9(1)$ mm (radius at $1/e^2$), truncated by a circular diaphragm of diameter $D = 20.3(1)$ mm. This diaphragm sets the maximal numerical aperture to $\mathrm{NA} = \sin(\theta_{\max}) = 0.55(2)$.

In this configuration a so-called Fourier speckle pattern is formed around the position of the atoms. In order to characterize it, the random intensity pattern was recorded at the position of the atoms with an high-resolution optical microscope, see Fig. **??**(b). As can be seen, the laser speckle field is very elongated along the propagation axis (x direction), resulting in a quasi-2D potential.

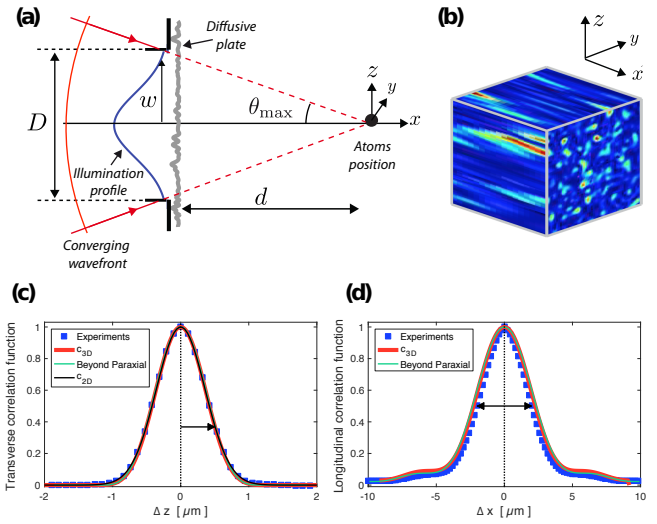

FIG. 2. **Laser speckle characterization.** (a) Schematic representation of the experimental configuration used for the speckle generation, with $\mathrm{NA} = \sin(\theta_{\max}) = 0.55(2)$. (b) 3D representation of the experimental laser speckle field. (c) Transverse correlation function along the z direction (same along y). Blue squares: experimental measurement c_{exp} from the recorded intensity pattern. Black solid line: transverse Gaussian fit $c_{2\mathrm{D}}$, yielding $\sigma = 0.50(1)\,\mu$m ($1/e$ radius). Red solid line: effective paraxial calculations $c_{3\mathrm{D}}$ (see text). Green solid line: beyond paraxial calculations, as done in Ref. **?** . This line is barely visible due to superposition with the effective paraxial model. (d) Longitudinal correlation functions with the same legend as in (c). The measured width is $\sigma_{\parallel} = 4.1(1)\,\mu$m (FWHM) .

Spatial statistical properties: measurement of the auto-correlation function

The normalized two-point correlation function of the laser speckle field,

$$c_{\mathrm{exp}}(\Delta\mathbf{r}) = \frac{\langle \delta I(\mathbf{r})\, \delta I(\mathbf{r}+\Delta\mathbf{r})\rangle}{\langle \delta I^2\rangle} \quad \text{with } \delta I = I - \langle I\rangle\,, \quad (1)$$

is directly calculated from the recorded spatial pattern shown in Fig. **??**(b). The resulting transverse and longitudinal correlation functions are respectively shown as blue squares in Fig. **??**(c) and (d).

In the transverse plane, the shape is found to be very close to a Gaussian. A fit of the form (solid black line):

$$c_{2\mathrm{D}}(\Delta\mathbf{r}_\perp) = e^{-\Delta\mathbf{r}_\perp^2/\sigma^2}\,, \quad (2)$$

realized either along the y or z axis, yields $\sigma = 0.50(1)\,\mu$m ($1/e$ radius).

The laser speckle field being very elongated, the correlation function has a much larger width in the longitudinal direction x. It is characterized by the FWHM $\sigma_{\parallel} = 4.1(1)\,\mu$m [see Fig. **??**(d)].

Modeling the laser speckle field

Due to the large numerical aperture $\mathrm{NA} = \sin(\theta_{\max}) = 0.55(2)$, the precise modeling of the speckle field requires in principle to go beyond the paraxial approximation. A theoretical model (not detailed here) was thus used in Ref. **?** to reproduce the measured correlation functions, see green solid lines in Fig. **??**(c) and (d).

However this theoretical model is quite heavy to handle, especially in view of the determination of the 3D spatial frequency distribution $\tilde{C}(\mathbf{k}_{\mathrm{dis}})$, a key quantity to calculate the Born prediction. Thus, we developed a simpler model, based on the paraxial approximation but including a global geometrical factor x_{scale} to tune the numerical aperture. In this effective paraxial model, the correlation function can be calculated using Fourier Transform (FT) [**?**]:

$$c_{3\mathrm{D}}(\Delta\mathbf{r}_\perp, \Delta x) \propto \left| \mathrm{FT}\Big[\, t(\mathbf{R}_\perp)\, I_{\mathrm{inc}}(\mathbf{R}_\perp)\, e^{-i\pi \frac{R_\perp^2}{\lambda}\frac{\Delta x}{d}} \Big]_{\frac{\Delta\mathbf{r}_\perp}{\lambda d}} \right|^2, \quad (3)$$

where $\mathrm{FT}\big[\, f(x)\,\big]_u = \int_{-\infty}^{+\infty} dx\, f(x) e^{-2i\pi u x}$. Here $t = \mathrm{disc}\big[R_\perp/(D_{\mathrm{eff}})\big]$ represent the transmission of a circular diaphragm of diameter $D_{\mathrm{eff}} = x_{\mathrm{scale}}\, D$, and $I_{\mathrm{inc}} = e^{-2R_\perp^2/(w_{\mathrm{eff}})^2}$ is the Gaussian illumination profile on the diffuser, with effective waist $w_{\mathrm{eff}} = x_{\mathrm{scale}}\, w$.

Setting $x_{\mathrm{scale}} = 0.875(5)$ (resulting in an effective maximal numerical aperture $\mathrm{NA}_{\mathrm{eff}} = 0.5$), the calculated correlation function $c_{3\mathrm{D}}(\Delta\mathbf{r})$ matches also very well with the measurements, both on the transverse and longitudinal directions [see red solid lines in Fig. **??**(c) and (d)].

Thus, we used this effective paraxial model to calculate the Born prediction for our specific disorder configuration (see below).

Calibration of the disorder amplitude V_{R}

In practice, the disorder amplitude V_{R} can be calibrated by combining photometric measurements and calculation of the atomic polarizability [**?**]. However it is known that such method leads to systematic uncertainties, typically around a few tens of percents (see e.g. Refs. **?** **?**).

Here, we used the excellent agreement between the experimental determination of τ_{s} and the numerical simulations [see Fig. 2(b) of the main text] to precisely determine the disorder amplitude by applying an overall correction α on the photometric measurement. In practice, the correction factor is calculated by minimizing the differences between the experiments and numerics for the particular momenta $k_i = 0.74\,\sigma^{-1}$, leading to $\alpha = 1.29(2)$. We mainly attribute this correction to the difficulty to estimate precisely the extension of the speckle field at the position of the atoms.

FIRST ORDER BORN APPROXIMATION

Rescaled scattering times $\tilde{\tau}_{\mathrm{s}}^{\mathrm{Born}}$

An important feature of the Born prediction is the simple scaling $\tau_{\mathrm{s}}^{\mathrm{Born}} \propto 1/|V_{\mathrm{R}}|^2$ with the disorder amplitude. Indeed, the spatial frequency distribution of the disorder can be written in the form $\tilde{C}(\mathbf{k}_{\mathrm{dis}}) = |V_{\mathrm{R}}|^2 \tilde{c}(\mathbf{k}_{\mathrm{dis}})$, where $\tilde{c}(\mathbf{k}_{\mathrm{dis}})$ is the Fourier transform of the normalized correlation function $c(\Delta\mathbf{r})$ [as in Eq. (**??**) above]. The Born prediction [see Eq. (2) of the main text] can then be rewritten in the form:

$$\tau_{\mathrm{s}}^{\mathrm{Born}}(\mathbf{k}_i, V_{\mathrm{R}}) = \frac{\hbar E_{\mathrm{R}}}{\pi V_R^2} \cdot \tilde{\tau}_{\mathrm{s}}^{\mathrm{Born}}(\mathbf{k}_i) \tag{4}$$

where $E_{\mathrm{R}} = \hbar^2/m\sigma^2$ is the so-called correlation energy and $\tilde{\tau}_{\mathrm{s}}^{\mathrm{Born}}$ is the rescaled scattering time that gives the dependence with the momentum $\mathbf{k}_i$. Its expression relies on the integration of the normalized spatial frequency distribution $\tilde{c}(\mathbf{k}_{\mathrm{dis}}) = \tilde{c}(\mathbf{k}' - \mathbf{k}_i)$ over the elastic scattering sphere ($|k'| = |k_i|$) [**?** **?**]:

$$\tilde{\tau}_{\mathrm{s}}^{\mathrm{Born}}(\mathbf{k}_i) = \frac{4\pi^3\sigma^2}{|k_i| \int d\Omega_{\mathbf{k}'}\, \tilde{c}(\mathbf{k}' - \mathbf{k}_i)}, \tag{5}$$

3D Born prediction $\tilde{\tau}_{\mathrm{s,3D}}^{\mathrm{Born}}$

The rescaled Born prediction $\tilde{\tau}_{\mathrm{s,3D}}^{\mathrm{Born}}$ corresponding to our experimental configuration is shown in Fig. **??**. As said above, this calculation uses the effective paraxial model c_{3D} given by Eq. (**??**) to reproduce the measured two-point correlation function.

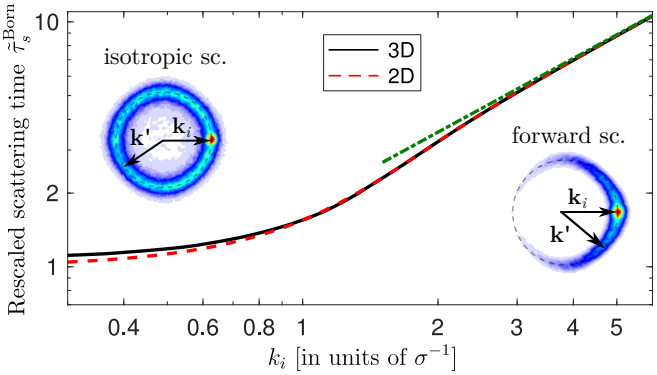

FIG. 3. **Rescaled Born prediction $\tilde{\tau}_{\mathrm{s}}^{\mathrm{Born}}$.** Black solid line: 3D Born prediction $\tilde{\tau}_{\mathrm{s,3D}}^{\mathrm{Born}}$ using the correlation $c_{\mathrm{3D}}(\Delta\mathbf{r})$ given by Eq. (**??**) (effective paraxial model). Red dashed line: 2D Born prediction $\tilde{\tau}_{\mathrm{s,2D}}^{\mathrm{Born}}$ for a transverse Gaussian correlation of size σ (1/e radius). Green dash-dotted line: asymptotic behavior at large momentum $\tilde{\tau}_{\mathrm{s}}^{\mathrm{Born}} \sim \sqrt{\pi} k_i \sigma$. Illustrations of the momentum distribution in the isotropic ($k_i \ll \sigma^{-1}$) and forward scattering ($k_i \gg \sigma^{-1}$) regimes are the same as in Fig. (1) of the main text.

Although the configuration is slightly different, the results discussed in Refs. **?** **?** for the case of a pure Gaussian illumination still hold for our case [**?**]. First, $\tilde{\tau}_{\mathrm{s,3D}}^{\mathrm{Born}}$ increases linearly with the momentum as $\sqrt{\pi} k_i \sigma$ in the large momentum limit ($k_i \gg \sigma^{-1}$), see dash-dotted green line in Fig. **??**. This behavior is generic for matter wave and does not depend on the dimension. Second, $\tilde{\tau}_{\mathrm{s,3D}}^{\mathrm{Born}}$ tends towards a constant in the low momentum limit ($k_i \ll \sigma^{-1}$). This behavior is specific to the laser speckle disordered potential [**?**]: it results from the absence of white noise limit due to the infinite correlation range in the longitudinal direction [**?**].

Comparison with 2D prediction $\tilde{\tau}_{\mathrm{s,2D}}^{\mathrm{Born}}$

The very elongated nature of the laser speckle field, having an infinite correlation range along the longitudinal direction, strongly suggests that our experiment can be described by a pure two-dimensional system. This is confirmed by the excellent agreement between the full 3D calculation $\tilde{\tau}_{\mathrm{s,3D}}^{\mathrm{Born}}$ and the Born prediction $\tilde{\tau}_{\mathrm{s,2D}}^{\mathrm{Born}}$ for a 2D disordered potential having a Gaussian correlation of size σ ($1/e$ radius). In the latter case, one has [**?** **?**]:

$$\tilde{\tau}_{\mathrm{s,2D}}^{\mathrm{Born}}(\mathbf{k}_i) = e^{k_i^2\sigma^2/2} / I_0(k_i^2\sigma^2/2)\ , \tag{6}$$

where I_0 is the zero-order modified Bessel function. $\tilde{\tau}_{\mathrm{s,2D}}^{\mathrm{Born}}$ tends towards 1 for low initial momentum ($k_i \ll \sigma^{-1}$) and, as expected, increases in the same way as the 3D case at large momentum ($\tau_{\mathrm{s}}^{\mathrm{Born}} \sim \sqrt{\pi} k_i \sigma$ for $k_i \gg \sigma^{-1}$).

NUMERICAL SIMULATIONS

The numerical calculations are performed by solving the Schrödinger equation for a particle of mass m in a 2D disordered potential $V(\mathbf{r})$. The initial state is a Gaussian wave packet of central momentum k_i and negligible momentum spread Δk [**?**]. The scattering time τ_s is extracted from the decay of the initial momentum distribution in the same way than for the experimental data (see Fig. **??**). The simulations are averaged over 14 different disorder realizations, which is found sufficient to achieve convergence.

To generate the disordered potential, we first calculate the field resulting from the convolution of a spatially uncorrelated complex random field, whose real and imaginary parts are independent Gaussian random variables, with a Gaussian profile accounting for the spatial correlations. The Gaussian-distributed potential is obtained by considering the real part of this field, leading to a Gaussian amplitude probability distribution. Instead, the laser speckle disordered potentials are obtained by considering the intensity (modulus square) of the resulting field [**?**], with a negative (resp. positive) sign for the attractive (resp. repulsive) disorder.

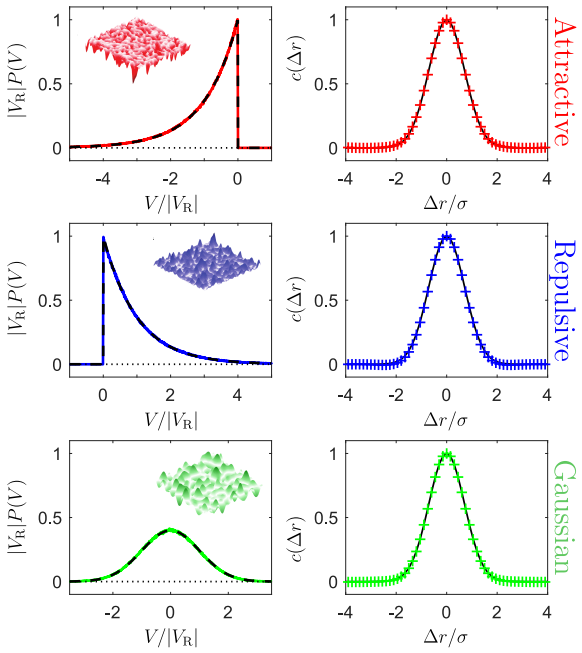

FIG. 4. **Numerically generated disorders.** The amplitude probability distribution $P(V)$ (left column) and the normalized correlation function $c(\Delta r)$ (right column) are shown for attractive (first row), repulsive (second row) and Gaussian-distributed (third row) disordered potentials. The amplitude probability distributions are in perfect agreement with the theoretical functions (black dashed lines), namely an exponential function for the attractive and repulsive disorders and a Gaussian function for the Gaussian disorder. The three disorders exhibit the same correlation function, which corresponds to a Gaussian function of size σ ($1/e$ radius).

In each case, we adjust the amplitude of the complex random field for the rms value of the probability distribution to be V_R. It yields $P(V) = |V_R|^{-1} e^{-V/V_R} \cdot \Theta(V/V_R)$, with Θ the step function, for the attractive and repulsive laser speckle fields (first and second rows in Fig.**??**), and $P(V) = (\sqrt{2\pi}V_R)^{-1} e^{-V^2/2V_R^2}$ for the Gaussian-distributed disorder (3rd row). In the same way, the spatial width of the Gaussian profile is adjusted in each case for the two-point correlation function of the disorder to be a Gaussian of size σ ($1/e$ radius), i.e., $c(\Delta r) = e^{-\Delta r^2/\sigma^2}$.

---

* Corresponding author: vincent.josse@institutoptique.fr

[] The initial momentum is not an inverted parabola — which is expected for a Bose Einstein condensate in the Thomas Fermi regime— but merely resembles to a Gaussian once the delta-kick cooling technique has been applied.

[] V. V. Volchkov, M. Pasek, V. Denechaud, M. Mukhtar, A. Aspect, D. Delande, and V. Josse, Phys. Rev. Lett. **120**, 060404 (2018).

[] J. W. Goodman, *Speckle phenomena in optics: theory and applications* (Roberts and Company, 2007).

[] D. Clément, A. F. Varón, J. A. Retter, L. Sanchez-Palencia, A. Aspect, and P. Bouyer, New Journal of Physics **8**, 1 (2006).

[] G. Semeghini, M. Landini, P. Castilho, S. Roy, G. Spagnolli, A. Trenkwalder, M. Fattori, M. Inguscio, and G. Modugno, Nat. Phys. **11**, 554 (2015).

[] J. Rammer, *Quantum Transport Theory*, Frontiers in Physics (Avalon Publishing, 2004).

[] E. Akkermans and G. Montambaux, *Mesoscopic physics of electrons and photons* (Cambridge University Press, 2007).

[] M. Piraud, L. Pezze, and L. Sanchez-Palencia, EPL (Europhysics Letters) **99**, 1 (2012).

[] M. Piraud, L. Pezzé, and L. Sanchez-Palencia, New Journal of Physics **15** (2013), 10.1088/1367-2630/15/7/075007.

[] In the case of a pure Gaussian illumination, i.e., for $D \to \infty$, the longitudinal correlation has a pure Lorentzian shape, and the 3D two-point correlation function reads:

$$c_{3D,\mathrm{Gauss}} = \frac{1}{1+4\Delta x^2/\sigma_{\parallel,\mathrm{Gauss}}^2}\, e^{-\frac{\Delta r_\perp^2/\sigma^2}{1+4\Delta x^2/\sigma_{\parallel,\mathrm{Gauss}}^2}}. \quad (7)$$

with $\sigma_{\parallel,\mathrm{Gauss}} = 4\pi\sigma^2/\lambda$.

[] In the case of a white noise limit, i.e., finite correlation range, the scattering time increases as $\propto 1/|k_i|$ in the low momentum limit.

[] B. Shapiro, Journal of Physics A: Mathematical and Theoretical **45**, 143001 (2012).

[] We have checked that this momentum spread has no influence on the extracted scattering time.